This peer-reviewed article has been accepted for publication in Publications of the Astronomical Society of Australia but not yet copyedited or typeset, and so may be subject to change during the production process.

The article is considered published and may be cited using its DOI. 10.1017/pasa.2025.10058

ASKAP–EMU radio continuum detection of planetary nebula NGC 5189: the "Infinity" nebula

A. D. Asher,[1,2] Z. J. Smeaton,[1] M. D. Filipović,[1] A. M. Hopkins,[3] J. Th. van Loon,[4] T. J. Galvin,[5] and L. A. Barnes[1]

[1]Western Sydney University, Locked Bag 1797, Penrith South DC, NSW 2751, Australia
[2]ATNF, CSIRO, Space and Astronomy, PO Box 76, Epping, NSW 1710, Australia
[3]School of Mathematical and Physical Sciences, 12 Wally's Walk, Macquarie University, NSW 2109, Australia
[4]Lennard-Jones Laboratories, Keele University, ST5 5BG, UK
[5]ATNF, CSIRO, Space and Astronomy, PO Box 1130, Bentley, WA 6151, Australia
Author for correspondence: A. D. Asher, Email: albany.asher@csiro.au.

Abstract

We report the radio continuum detection of well known Galactic Planetary Nebula (PN) NGC 5189, observed at 943 MHz during the Australian Square Kilometre Array Pathfinder (ASKAP) Evolutionary Map of the Universe (EMU) survey. Two detections of NGC 5189 have been made during the survey, of better resolution than previous radio surveys. Both measurements of the integrated flux density are consistent with each other, at $S_{943\,\mathrm{MHz}} = 0.33 \pm 0.03$ Jy, and the spectral luminosity is $L_{943\,\mathrm{MHz}} = 8.89 \times 10^{13}$ W m^{-2} Hz^{-1}. Using available flux density measurements for radio-detections of NGC 5189, we calculate a radio surface brightness at 1 GHz and measure $\Sigma_{1\,\mathrm{GHz}} = 6.0 \times 10^{-21}$ W m^{-2} Hz^{-1} sr^{-1}, which is in the expected range for Galactic PNe. We measure an apparent size of $3\farcm4 \times 2\farcm2$ corresponding to physical diameters of 1.48 pc × 0.96 pc, and combine available radio observations of NGC 5189 to estimate a spectral index of $\alpha = 0.12 \pm 0.05$. Hence, we agree with previous findings that NGC 5189 is a thermal (free–free) emitting nebula. Additional measurements of the optical depth ($\tau = 0.00246$) and electron density ($N_e = 138\ cm^{-3}$) support our findings that NGC 5189 is optically thin at 943 MHz. Furthermore, the radio contours from the ASKAP–EMU image have been overlaid onto a *Hubble Space Telescope* (HST) Wide Field Camera 3 image, demonstrating that the radio morphology closely traces the optical. Notably, the contour alignment for the innermost region highlights the two envelopes of gas previously reported to be low-ionisation structures, which is considered a defining feature of post common–envelope PNe that surround a central Wolf-Rayet star.

Keywords: Planetary nebulae; Galactic radio sources; Radio-continuum emission; Radio astronomy

1. INTRODUCTION

Planetary nebulae (PNe) are shells of gas that are shed during the terminal phase for the majority of stars between ∼1–8 $M_\odot$ (Pottash, 1983; Gathier et al., 1986), when they transition from the asymptotic giant branch (AGB) to the white dwarf stage (Kwok, 2005). The transitioning star ionises the surrounding shells and these remain visible for thousands of years, providing crucial insight into the recent mass loss rate, mechanism and nucleosynthesis of the AGB star, as well as the evolution of the parent galaxy (particularly the chemical and star-forming evolution) (Kwok, 2005; Gesicki et al., 2018; Crawford, 2015).

NGC 5189 is a well known Galactic PN located in the southern constellation Musca at RA (J2000) 13:33:31.8 and DEC (J2000) –65:58:29.8, at a distance of ∼1500 parsecs (Chornay & Walton, 2021). It was discovered by Scottish astronomer James Dunlop in 1826 (Dunlop, 1828; Cozens et al., 2010) during observations from Parramatta, Australia, using a 9-inch reflector telescope[a]. However, it was not considered a PN until more recently by Evans & Thackeray (1950) (an optical study), which they describe as "clearly not an ordinary planetary" and at the time they did not observe any central star. It was later determined to be a quadrupolar PN with multiple sets of "symmetrical condensations" (ansae, or knots) by Sabin et al. (2012) (both an optical and infrared study), and first identified as a binary system by Manick et al. 2015, where the central Wolf–Rayet [WO1] star (Crowther et al., 1998) is in a binary orbit with potentially a main-sequence star or a white dwarf (Manick et al., 2015).

NGC 5189 is renowned for its complex morphology and has been described by a number of authors (e.g. Sabin et al. 2012; Danehkar et al. 2018; Aller et al. 2020) as having filamentary and knotty structures, which can be attributed to the central binary system. A subsequent study by Bear & Soker (2017), however, suggests the structure may result from a ternary (triple) progenitor system (Danehkar et al., 2018). According to Phillips & Reay (1983), the symmetrical condensations that NGC 5189 distinctly exhibits are the result of precessional torque induced by the companion star as it orbits the central star.

1.1 Radio Observations of PNe

Radio continuum observations of PNe are not only useful for measuring the integrated flux densities and the associated spectral index, but also for tracing the thermal emission from the ionised plasma shells (Hajduk et al., 2018) and determining the PN geometry and structures without the impediment of

[a]We refer the interested reader to James's original representation of NGC 5189 (catalogued as object #252) in Dunlop (1828).

https://doi.org/10.1017/pasa.2025.10058 Published online by Cambridge University Press

interstellar and atmospheric extinction (Zijlstra et al., 1994). While radio continuum surveys generally report the detection of weak thermal free–free emission from a PN (Asher et al., 2024; Filipović et al., 2009; Gathier et al., 1983; Milne & Aller, 1982; Pennock et al., 2021), a few studies have reported non-thermal detections in the early photoionisation phase, as AGB stars transition to the white dwarf stage (Bains et al., 2009; Cerrigone et al., 2017; Pérez-Sánchez et al., 2013; Suárez et al., 2015). A notable example is the Hajduk et al. (2024) study regarding the radio continuum emission from Sakurai's Object (V4334 Sgr), the central star of a PN (CSPN) in the Sagittarius constellation. The authors observed the source between 2004 and 2023, finding non-thermal and highly variable emission to dominate between 2004 and 2017. This indicates Sakurai's object is a proto-PNe (or pre-planetary nebulae [PPN], Kwok 2001) in the early photoionisation phase, of which the authors attribute the non-thermal emission to the shock interactions during mass-ejection events, as stellar winds from the AGB star interact with the PN shell (Hajduk et al., 2024).

Slee & Orchiston (1965) were the first to observe NGC 5189 in the radio spectrum, at both 1420 MHz and 2700 MHz with the Parkes 64-m telescope. Subsequent Parkes radio detections (Table 1) were made between 1972 and 1982 at frequencies ranging from 2700 MHz to 14.7 GHz (Aller & Milne, 1972; Milne & Aller, 1975; Milne, 1979; Milne & Aller, 1982).

More recent detections were made in 1990 at 4850 MHz during the Parkes-MIT-NRAO (PMN) radio continuum survey (Griffith & Wright, 1993; Wright et al., 1994; Condon et al., 1993) (conducted by the Parkes telescope and using the National Radio Astronomy Observatory (NRAO)-developed seven-beam receiver, Condon et al. 1989) and in 2007 at 843 MHz during the second epoch Molonglo Galactic Plane Survey (MGPS-2) (Murphy et al., 2007) – the Galactic counterpart to the Sydney University Molonglo Sky Survey (SUMSS) (Bock et al., 1999; Mauch et al., 2003) by the Molonglo Observational Synthesis Telescope (MOST) (Mills, 1981; Robertson, 1991).

We liken the appearance of the central region of NGC 5189 to the lemniscate symbol, and hence our use of the colloquial moniker, *Infinity* for this object. Given the dearth of radio continuum measurements of *Infinity* (hereafter used interchangeably with NGC 5189) in recent years our primary goal has been to observe it and contribute up-to-date measurements using the ASKAP radio telescope array. Therefore, in this paper we present the most recent radio continuum measurements for *Infinity*, observed at 943 MHz during the ASKAP Evolutionary Map of the Universe (EMU) survey.

The paper is structured as follows. In §2 we describe the ASKAP–EMU radio data and respective processes used to determine the new radio continuum measurements, in addition to detailing the corresponding HST data used for comparative purposes. In §3 we present the flux density, spectral index and associated results, and we summarise our findings in §4.

2. DATA

2.1 ASKAP and the Evolutionary Map of the Universe Survey

The Evolutionary Map of the Universe survey (Norris et al., 2011; Hopkins et al., 2025) is a wide-field radio continuum galaxy survey being conducted by the ASKAP radio telescope (Johnston et al., 2008; Hotan et al., 2021), observing at the central frequency of 943 MHz and a bandwidth of 288 MHz (Hopkins et al., 2025). The EMU survey (ASKAP project AS201) began in May 2023 and will cover the entire southern sky by the scheduled time of completion in 2028 (Hopkins et al., 2025). The ASKAP array consists of 36 12-m antennas, with baselines up to 6 km, and has a large instantaneous field of view (ranging between 15 $\deg^2$ at 1700 MHz to 31 $\deg^2$ at 800 MHz) (Hotan et al., 2021).

Infinity has been observed twice during the EMU survey, with both observations using all 36 antennas over a duration of 10 hours. The respective scheduling blocks are SB53310 (observed on 30 September 2023) and SB62225 (observed on 7 May 2024). Both tiles are accessible via the CSIRO ASKAP Science Data Archive (CASDA)[b]. All EMU data is processed through the ASKAPsoft pipeline (Guzman et al., 2019).

Both images of *Infinity* (see Figure 1, top) have a resolution of 15.0×15.0 arcseconds^2, as well as a Stokes I image root mean squared (rms) noise value of 39 μJy beam^{-1}. For comparison, the median Stokes I image rms noise value of each scheduling block (across the full tile) is 40 μJy beam^{-1} (SB53310) and 44 μJy beam^{-1} (SB62225), of which the sky area is 41.42 and 41.57 $\deg^2$ respectively.

The data was predominantly analysed using the `CARTA` (Comrie et al., 2021) software, to establish the integrated flux densities for *Infinity*. The flux density measurements are presented in Table 1, in addition to measurements for the Parkes, PMN, SUMSS and MGPS-2 radio observations. For the PMN observation, we relied upon the `MIRIAD` (Sault et al., 1995, 2011) and `KARMA` (Gooch, 1996) software packages to measure the integrated flux density and uncertainty level, as a consequence of statistical issues experienced when scaling the image in `CARTA` (discussed further in §3).

Numerous flux density measurements have been achieved and investigated in a number of ASKAP–related papers, which we refer the interested reader to: including the Large Magellanic Cloud (LMC) Odd Radio Circle (ORC) J0624–6948 (Filipović et al., 2022; Sasaki et al., 2025); the Galactic supernova remnant (SNR) G278.94+1.35 (named "Diprotodon") by Filipović et al. (2024); the discovery of a new, young, Galactic SNR G329.9–0.5 ("Perun") by Smeaton et al. (2024b); the detection of a large and low surface brightness Galactic SNR G288.8–6.3 ("Ancora") by (Filipović et al., 2023) (with a follow-up study by Burger-Scheidlin et al. (2024)); and others (e.g. Lazarević et al. 2024; Smeaton et al. 2024a; Filipovic et al. 2025).

[b] https://research.csiro.au/casda/

https://doi.org/10.1017/pasa.2025.10058 Published online by Cambridge University Press

2.2 HST Data

We also use the available HST data from the Hubble Legacy Archive (HLA)[c] to compare the optical and radio properties. The images are from project 12812 (PI: Z. Levay), taken on 6 July 2012 using the Wide Field Camera 3 (WFC3) instrument[d] (Leckrone et al., 1998). We make use of three images to create a composite RGB image (Figure 1, bottom), specifically the F673N (red), a narrow-band filter centred at 676.59 nm with a width of 11.78 nm (which covers the [S II] doublet), F606W (green), a wide V band filter centred at 588.92 nm with a width of 218.92 nm (which covers the [O III] doublet [both lines] and the Hα line), and F502N (blue), a narrow-band filter centred at 500.96 nm with a width of 6.53 nm (which covers the red [O III] line). We use these images for comparison with radio, and an in-depth optical emission line analysis using the same data can be found in Danehkar et al. (2018).

3. RESULTS AND DISCUSSION

Flux density measurements of Galactic PNe are too varied to derive a suitable expectation for a single PN, which is not surprising given the variation in PN distances (the exception to this issue are the Magellanic Clouds (MC) PNe, which remain unresolved, Pennock et al. 2021). Based on the variation, we contribute supplementary measurements of the spectral luminosity[e] at 943 MHz, and the distance-independent radio surface brightness, Σ, at 1 GHz (a standard scaling frequency for determining surface brightness values, e.g. Cotton et al. 2024) and determine if the value falls in the expected range for Galactic PNe.

We also explore a historical comparison of flux density values. Historically, the values for *Infinity* have been measured between 0.215 Jy at 4850 MHz (Griffith & Wright, 1993; Wright et al., 1994) and 0.459 Jy at 14700 MHz (Milne & Aller, 1982). Using `CARTA` and the polygon tool to define the outline of *Infinity*, we measured an integrated flux density of $S_{943\,\mathrm{MHz}}$ = 0.333 Jy (SB53310) and $S_{943\,\mathrm{MHz}}$ = 0.334 Jy (SB62225). The `CARTA` software does not specifically provide uncertainty levels, however the `MIRIAD IMFIT` task does, available from the `MIRIAD` (Sault et al., 1995, 2011) software package developed by the Australia Telescope National Facility (ATNF). Two separate assessments of the *Infinity* images indicate an uncertainty level of $\sim$10% for both images. The ASKAP measurements are presented in Table 1, in addition to the historical flux density values and their respective uncertainties.

In respect to the apparent size of *Infinity*, using `CARTA` and retaining the polygon outline, we measured the angular dimensions of $3\farcm4 \times 2\farcm2$. Using the Chornay & Walton (2021) distance of $\sim$1500 pc in our calculation, this corresponds to a physical size of 1.48 pc $\times$ 0.96 pc. Using the same distance of $\sim$1500 pc, we measure the spectral luminosity, $L_{943\,\mathrm{MHz}} = 8.89 \times 10^{13}$ W m^{-2} Hz^{-1}.

We also employ the mean of the angular dimensions to determine the surface brightness of *Infinity* at 1 GHz, of which we measure 6.0×10^{-21} W m^{-2} Hz^{-1} sr^{-1}. This value falls within the expected range of radio surface brightnesses for Galactic PNe (between $\sim 10^{-24} - 10^{-16}$ W m^{-2} Hz^{-1} sr^{-1}, Leverenz et al. 2016), again placing confidence in the measurements.

Additionally, we measured the integrated flux densities of *Infinity* in the SUMSS and PMN surveys. The reason for measuring SUMSS is that the integrated flux density value for *Infinity* is not present in the respective catalogue. For the PMN observation, there are two different measurements presented in the catalogue (where *Infinity* is listed in the final source catalogue, "Table 2" in Wright et al. (1994) and Table 2 in the online point source catalogue [f], as per its J2000–derived source name, J1333–6558). The two measurements are $S_{4850\,\mathrm{MHz}} = 0.309\pm0.017$ Jy and $S_{4850\,\mathrm{MHz}}$ = 0.215 Jy, respectively. Initially, we considered that the latter measurement may have resulted from measuring a steep spectral source, as the value is not in close agreement with the majority of historical observations. However, Wright et al. (1994) explain that a few complex objects were larger than the beam size and led to multiple measurements of those sources being included in Table 2. The measurement of 0.215 Jy was determined using a "General-width fit" (Griffith & Wright, 1993), designed for detecting and measuring extended sources, where the maximum and minimum widths of a source are normalised to the beam size of $4\farcm2$. This method may explain the discrepancy between the two measurements. Regardless, we choose to measure the PMN *Infinity* detection again.

We accessed the respective FITS files via SkyView[g] and analysed accordingly in `CARTA`, assuming a 10% uncertainty level as described and investigated in the aforementioned ASKAP–related studies (see §2.1). For the 843 MHz image in the SUMSS survey, we measured an integrated flux density of 0.245 ± 0.025 Jy. We note that `CARTA` did not generate the integrated flux density directly (due to missing information in the image file header, most notably the restoring beam and frequency), but rather we used `CARTA's` *Sum* flux value of the selected region, 4.644 Jy, to determine the integrated flux density using the following formula (Filipovic, 1996):

$$S_\nu = \frac{\mathrm{Sum}}{1.133(\frac{BS}{PS})^2}\,, \tag{1}$$

where S_ν is the integrated flux density at a given frequency, *Sum* is the flux value of the selected region (in Jy), *BS* is the beam size (for SUMSS this is $45'' \times 45''$) and *PS* is pixel size (for SUMSS this is $11'' \times 11''$).

For the 4850 MHz image in the PMN survey, limited header information in the image file prevented measurements using `CARTA`. Therefore, we employed `MIRIAD IMFIT` and

[c] https://hla.stsci.edu/

[d] Refer to the WFC3 Instrument Handbook (Marinelli & Green, 2024) for further information on UVIS imaging with WFC3: https://hst-docs.stsci.edu/wfc3ihb

[e] We assume an isotropic source when using the formula $L_\nu = 4\pi d^2 S_\nu$, where ν is the ASKAP–EMU frequency and d is the Chornay & Walton (2021) distance to *Infinity* in metres (Marr et al., 2015).

[f] The PMN point source catalogues and survey maps can be accessed at: https://www.parkes.atnf.csiro.au/observing/databases/pmn/pmn.html

[g] https://skyview.gsfc.nasa.gov

https://doi.org/10.1017/pasa.2025.10058 Published online by Cambridge University Press

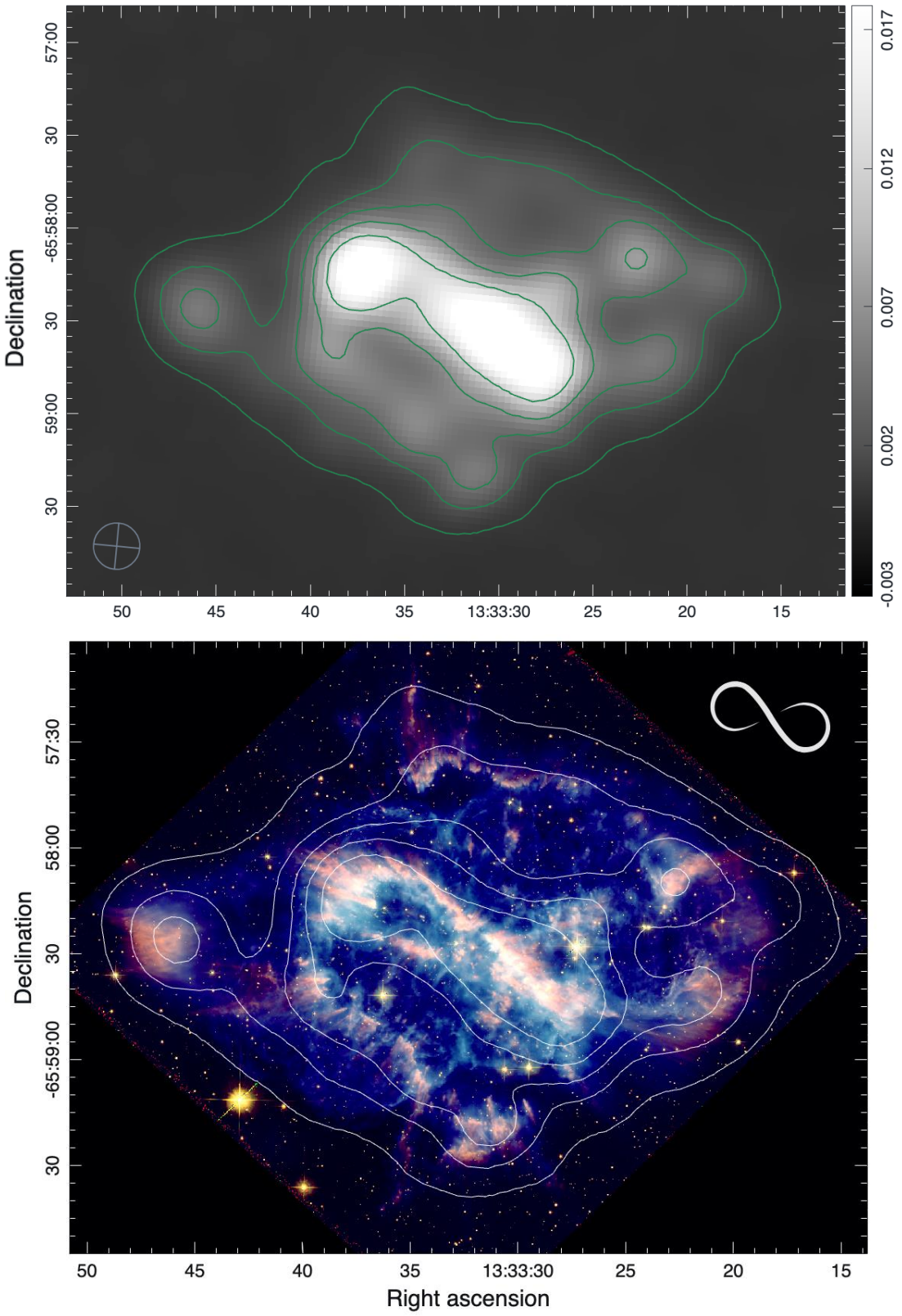

Figure 1. **Top:** ASKAP–EMU radio image of *Infinity* at 943 MHz with an rms noise level of 39 μJy beam^{-1}. The contours are at levels of 10, 50, 100, 175, and 200σ. The synthesised beam size is shown in the bottom left corner. **Bottom:** RGB image of *Infinity* from HST images, overlaid with ASKAP–EMU radio image contours. Red is the F673N filter (a narrow-band filter centred at 676.59 nm), green is the F606W filter (a wide V band filter centred at 588.92 nm), and blue is the F502N filter (a narrow-band filter centred at 500.96 nm). All images are from the WFC3 instrument.

https://doi.org/10.1017/pasa.2025.10058 Published online by Cambridge University Press

determined a flux density value of 0.310±0.004 Jy, which is in close agreement with the value listed in the final source catalogue in Wright et al. (1994). The PMN[h] and SUMSS measurements are also presented in Table 1.

Importantly, when analysing the PMN *Infinity* observation in CARTA, we created an ellipse region to represent the boundary of the second measurement (as per the 4.′2 beam size) and applied to both the ASKAP–EMU and PMN images. In Figure 2, the normalised PMN region of 4.′2 × 4.′2 is indicated by the cyan ellipse in both images (to the left is PMN and to the right is ASKAP–EMU, where both intensity scales are measured in Jy/beam). For comparison, the central region observed by ASKAP is indicated by the pink polygon. In the ASKAP–EMU image, there are a number of background sources that fall within the PMN-catalogued region. Upon assessment of the four most distinct background sources (which have a combined integrated flux value of ∼0.0024 Jy), it is reasonable to conclude that they have a negligible effect, despite being included in the measurement. Additionally, we would expect steep spectral sources observed at 4850 MHz to be fainter than observations at ∼1 GHz. The reason the second measurement is lower is therefore unclear.

In Figure 3, we estimate the spectral index using 11 of the 12 radio data points listed in Table 1. Only one of the PMN measurements can be included in the calculation, to correspond with one observation, of which we employ the value listed in the final source catalogue (Wright et al., 1994). We estimate a spectral index[i] of $\alpha = 0.12 \pm 0.05$. Thermal free–free emission is typically associated with spectral indices of $\alpha = 0 - 2$ and non-thermal with $\alpha < -0.5$ (Ridpath, 2018). Accordingly, we infer that NGC 5189 is a thermal (free–free) emitting nebula. This finding agrees with previous observations (e.g. Aller & Milne 1972; Milne & Aller 1982).

Inspection of the data in Figure 3 shows that the three data points at lower frequencies (<1000 MHz in this instance, i.e. SUMSS, MGPS-2, ASKAP–EMU) indicate a small degree of brightening over a 21–year period (from 0.245 Jy at 843 MHz [SUMSS] up to 0.334 Jy at 943 MHz [ASKAP–EMU]), although this is marginal. Based on the combination of age, differing flux scales and measurement techniques, the Parkes (1965a) and PMN (1994) data points are likely to be outliers; with emphasis on the differing flux density scales, as both sets of observations were determined using the radio galaxy Hydra-A (PKS B0915–118) to calibrate the absolute flux density scale (Slee & Orchiston, 1965; Condon et al., 1993). For comparison, ASKAP employs radio galaxy PKS B1934–638 to calibrate the absolute flux density scale (Hotan et al., 2021).

The data point at 14.7 GHz (Milne & Aller, 1982) is slightly higher than the others, yet in agreement with an earlier Parkes observation at 5 GHz (Milne, 1979), and certainly within the uncertainty level of the 1979 observation. Milne & Aller (1982) compared the 14.7 GHz and earlier 5 GHz flux density measurements (Milne, 1979) for 236 confirmed PNe (including *Infinity*) and found there to be notable scattering in the diagram. They mostly attribute this to the fixed error when measuring flux densities, in addition to the fractional error associated with calibration.

The remaining data points at higher frequencies (≥2700 MHz) show more consistency with little indication of variation with time. There is a marginal drop in flux density between the 1965b and 1972 Parkes observations at 2700 MHz, from 0.360 Jy to 0.330 Jy, respectively, but a similarly sized marginal increase in flux density at 5000 MHz between the 1975 and 1979 Parkes observations, although in both cases these are within the estimated uncertainties. The gap between the earliest (Parkes) and most recent (ASKAP) observations is six decades, and any temporal variation in flux density or spectral index on such a timeframe for this class of object is likely to be small.

According to Hajduk et al. (2018), flux evolution is not only dependent on factors such as age (where, for example, electron densities will generally decline monotonically as the PNe expands, Zhang et al. 2004) but also the central star's evolution, which vary in their progress and can contribute to variation in flux measurements.

Given the spectral index value of *Infinity* lies closer to the optically thin case of $\alpha = -0.1$ than the optically thick at $\alpha = 0.6 - 2.0$ (where more light is absorbed) (Taylor et al., 1987; Gruenwald & Aleman, 2007), we also infer that *Infinity* is predominantly within the optically thin regime for observations ≳1000 MHz.

To explore this result further, we rewrite the Rayleigh-Jeans approximation[j] so we can measure the optical depth, τ, which is proportional to the emission measure (EM) (defined as the integral of the electron density, N_e, along the line of sight in an emission nebula, Wilson et al. 2013):

$$S_\nu = \frac{2k\nu^2}{c^2} T_B \Delta\Omega \,, \tag{2}$$

where S_ν is the integrated flux density at a specific frequency, k is the Boltzmann constant, c is the speed of light, T_B is the brightness temperature and $\Delta\Omega$ is the angular area (measured as an elliptical area in this instance, equating to 4.971×10^{-7} sr). We rearrange Eq. 2 to solve for T_B:

$$T_B = \frac{S_\nu c^2}{2k\nu^2 \Delta\Omega} \,. \tag{3}$$

We measure $T_B = 24.6$ K. Brightness temperature can also be expressed as $T_B = T(1 - e^{-\tau})$, which we rearrange to solve for τ:

$$\tau = -ln\left(1 - \frac{T_B}{T}\right) \,. \tag{4}$$

We measure $\tau = 0.00246$. Since $\tau \ll 1$, this reinforces the conclusion that *Infinity* is optically thin at 943 MHz. To determine

[h]For the original PMN *Infinity* detection, we present the final source catalogue value (Wright et al., 1994) in Table 1 only.

[i]Spectral index is defined as $S \propto \nu^\alpha$, where S is integrated flux density, ν is observing frequency, and α is spectral index.

[j]The approximation is suitable to use as it holds for frequencies $\frac{\nu}{\mathrm{GHz}} \ll 21 \left(\frac{T}{K}\right)$ (Wilson et al., 2013).

https://doi.org/10.1017/pasa.2025.10058 Published online by Cambridge University Press

Table 1. We present the available flux density measurements for radio-detections of NGC 5189 (Column 4), in chronological order. *Year of catalogue release, excepting ASKAP–EMU, which are years of observation. †Average integrated flux density measurements, based on the average of 8 or 9 scans of *Infinity*, conducted by the Parkes telescope (8 scans for observations at 2700 MHz and 9 scans at 1420 MHz). ‡New integrated flux density measurements of existing radio data.

Year*	Telescope/Survey	ν (MHz)	$S \pm \Delta S$ (Jy)	Beam Size	References
1965	Parkes 64-m	1420	0.410±0.021†	14.′0 × 14.′0	Slee & Orchiston (1965)
1965	Parkes 64-m	2700	0.360±0.018†	7.′5 × 7.′5	Slee & Orchiston (1965)
1972	Parkes 64-m	2700	0.330±0.100	8.′1 × 8.′1	Aller & Milne (1972)
1975	Parkes 64-m	5000	0.366±0.025	4.′5 × 4.′5	Milne & Aller (1975)
1979	Parkes 64-m	5000	0.413±0.045	4.′5 × 4.′5	Milne (1979)
1982	Parkes 64-m	14700	0.459±0.023	2.′1 × 2.′1	Milne & Aller (1982)
1994	Parkes–MIT–NRAO	4850	0.309±0.017	4.′2 × 4.′2	Wright et al. (1994)
1994	Parkes–MIT–NRAO	4850	0.310±0.004‡	4.′2 × 4.′2	This paper, based on Wright et al. (1994).
2003	MOST–SUMSS	843	0.245±0.025‡	45 × 45 csc |δ| arcsec^2	This paper, based on Mauch et al. (2003).
2007	MOST–MGPS–2	843	0.307±0.012	45 × 45 csc |δ| arcsec^2	Murphy et al. (2007)
2023	ASKAP–EMU	943	0.333±0.033	15″ × 15″	This paper.
2024	ASKAP–EMU	943	0.334±0.033	15″ × 15″	This paper.

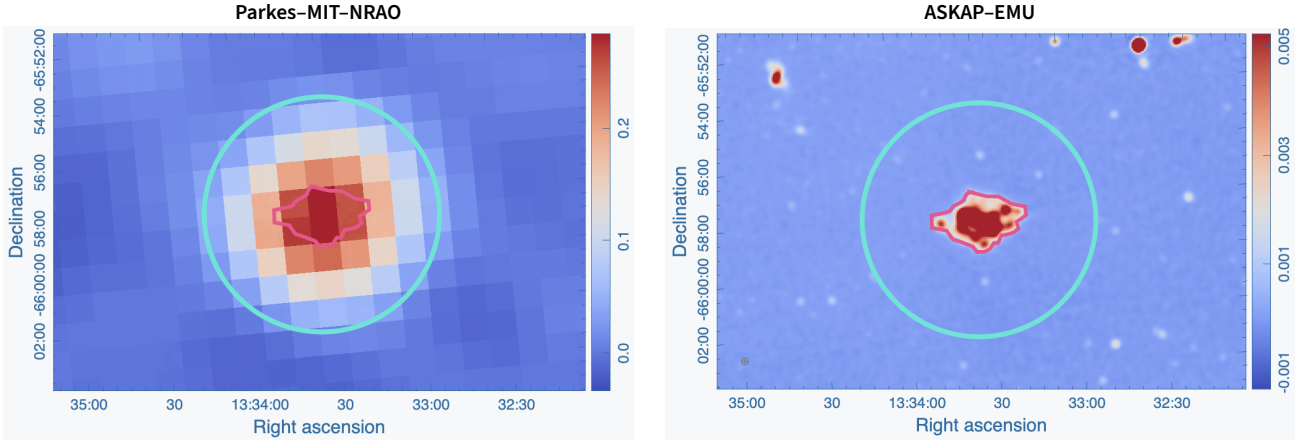

Figure 2. A comparison of *Infinity* observations: the cyan ellipse in both the PMN and ASKAP–EMU images represents the region that was measured during the PMN survey (Griffith & Wright, 1993; Wright et al., 1994; Condon et al., 1993). The central pink polygon in both images represents the *Infinity* PN from the recent ASKAP observations.

the EM and N_e values, we employ the Mezger & Henderson (1967) approximation for the free-free opacity τ:

$$\tau = 3.28 \times 10^{-7} \left(\frac{T}{10^4 K}\right)^{-1.35} \left(\frac{\nu}{GHz}\right)^{-2.1} \left(\frac{EM}{\text{pc cm}^{-6}}\right), \quad (5)$$

where for T we use the canonical value (10^4 K) (Bojičić et al., 2021), and ν is the frequency of the ASKAP–EMU survey in GHz (0.943). We then rearrange Eq. 5 and solve for EM specifically:

$$EM = \frac{\tau}{3.28 \times 10^{-7} \left(\frac{T}{10^4 K}\right)^{-1.35} \left(\frac{\nu}{GHz}\right)^{-2.1}}. \quad (6)$$

We measure $EM = 6630\,\text{pc cm}^{-6}$. From the following EM formula (Wilson et al., 2013) we can now rearrange and measure N_e:

$$EM = \int_0^s \left(\frac{N_e}{cm^3}\right)^2 d\left(\frac{s}{\text{pc}}\right) \quad (7)$$

$$\therefore \frac{N_e}{cm^3} = \sqrt{\frac{EM}{\left(\frac{s}{pc}\right)}}. \quad (8)$$

where overall this represents the integral of the electron density squared (N_e^2) at a depth (s) measured in pc. To determine the depth, we assume a cylindrical geometry and a path length equal to the smallest diameter of 2.′2. We measure $N_e = 138\,\text{cm}^{-3}$. Optically thin PNe have electron densities $<5000\,\text{cm}^{-3}$, whereas for optically thick PNe the electron densities are $>6000\,\text{cm}^{-3}$ (Barlow, 1987). Therefore, our result supports our earlier findings that *Infinity* is optically thin at 943 MHz.

https://doi.org/10.1017/pasa.2025.10058 Published online by Cambridge University Press

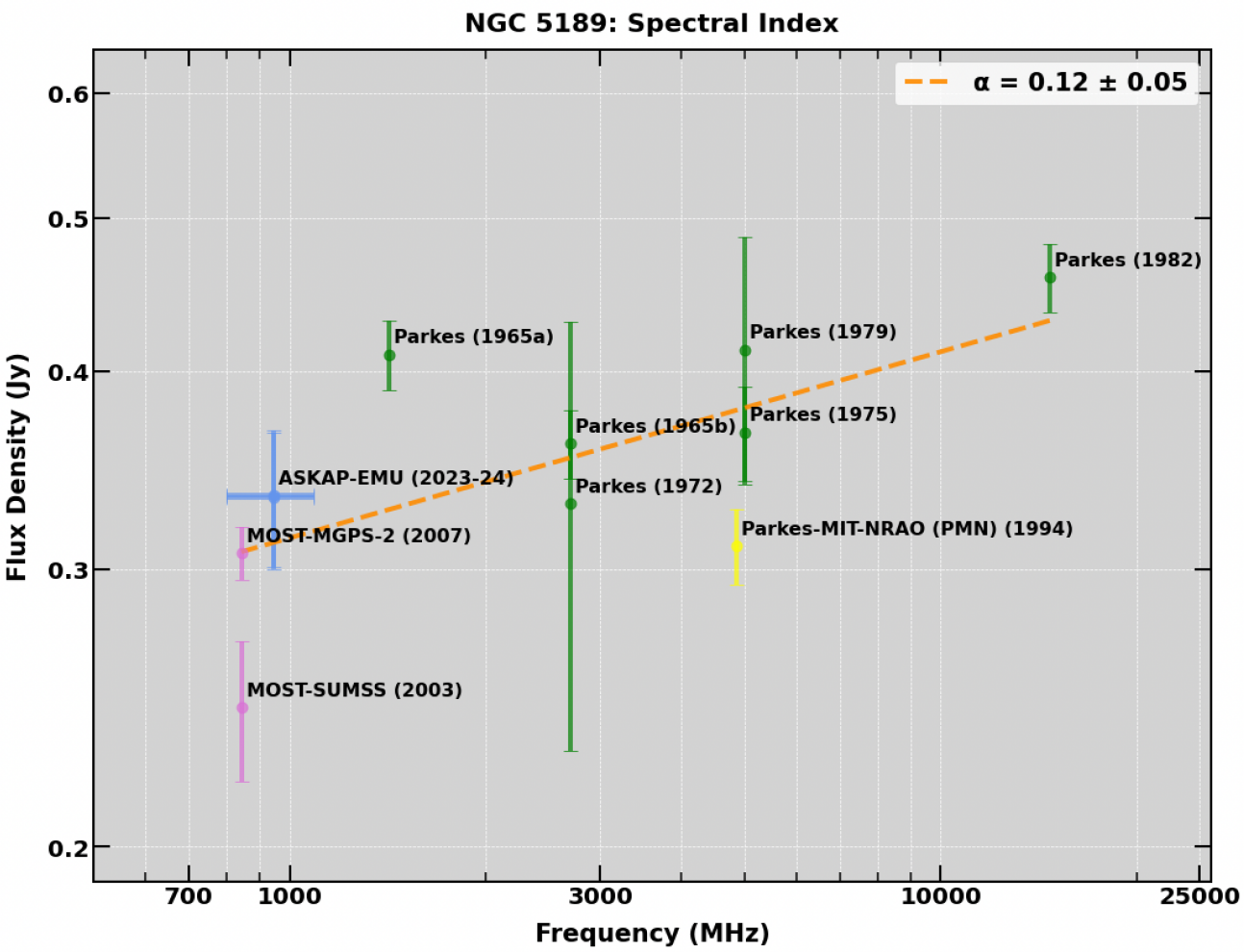

Figure 3. Using 11 of the 12 available radio data points (labelled according to the respective telescope and year of the associated paper or observation), we calculated the radio spectral index for *Infinity* and determined $\alpha = 0.12 \pm 0.05$, represented by the dashed orange line. Both axes are log scale. For the two ASKAP-EMU data points coloured blue, the survey bandwidth of 288 MHz has been marked with a horizontal line of the same colour.

Notably, from Figure 1 it is evident that the radio continuum emission closely follows the optical. Specifically, the radio emission closely traces the F606W filter. This is possibly due to the Hα emission line at 656.3 nm, which has a throughput close to the peak of the integrated system, ∼29%. Hα is related to the distribution and density of thermally-emitting ionised gas (Tacchella et al., 2022). Therefore, it provides valuable insight into the structure and morphology of PNe.

We use `CARTA` and the polygon tool to define the outline of the two inner envelopes in *Infinity's* central region, which we arbitrarily refer to as regions R1 and R2 in Figure 4 (measured in Jy/beam). The central coordinates for R1 are RA (J2000) 13:33:37.2 and DEC (J2000) –65:58:14, where we measured an integrated flux density of $S_{943\,\mathrm{MHz}} = 0.0312$ Jy (SB53310) and $S_{943\,\mathrm{MHz}} = 0.0315$ Jy (SB62225). The central coordinates for R2 are RA (J2000) 13:33:30.0 and DEC (J2000) –65:58:36, where we measure an integrated flux density of $S_{943\,\mathrm{MHz}} = 0.0696$ Jy (SB53310) and $S_{943\,\mathrm{MHz}} = 0.0698$ Jy (SB62225).

We measure the apparent size of the inner region containing only the R1 and R2 envelopes (indicated by the central black rectangle in Figure 4), which is $1\farcm6 \times 0\farcm52$, corresponding to a physical distance of 0.70 pc × 0.23 pc. Individually, the apparent size of the R1 envelope is $0\farcm48 \times 0\farcm37$, corresponding to a physical distance of 0.21 pc × 0.16 pc. For the R2 envelope, we measure $0\farcm85 \times 0\farcm42$, corresponding to a physical distance of 0.37 pc × 0.18 pc.

Using the mean of each of the R1 and R2 integrated flux density values, we also measure the optical depth and electron density values for these two inner envelopes, using the same methodology in equations 2 to 8 inclusive (this includes assuming a cylindrical geometry and hence measuring a path length equal to the smallest diameter, which for R1 is 0.16 pc and for R2 is 0.18 pc). This approach will determine whether *Infinity* becomes optically thick in the line of sight to the central region, which would not only impact the overall integrated flux density measurement but possibly explain why the spectral index value is slightly higher than the optically thin case of $\alpha = -0.1$. For R1 we measure $\tau = 0.0098$ and $N_e = 405.82\,\mathrm{cm}^{-3}$, and for R2 we measure $\tau = 0.011$ and $N_e = 402.66\,\mathrm{cm}^{-3}$. We can infer from both results of τ and N_e that *Infinity* is opti-

https://doi.org/10.1017/pasa.2025.10058 Published online by Cambridge University Press

cally thin in the R1 and R2 regions. In terms of the slightly raised spectral index value, this warrants further investigation in future research, particularly at lower frequencies where the optical thickness may not be negligible in a specific direction.

Danehkar et al. (2018) mapped the excitation in the inner regions using HST WFC3 imaging and describe the innermost structures as two low-ionisation envelopes (hence, spectroscopic studies predominantly detect emission lines such as [N II] and [O I], Mari et al. 2023) surrounded by highly ionised environments, resulting from recent outbursts of the progenitor AGB star. According to Miszalski et al. (2009), these low–ionisation structures are a defining feature of post common–envelope PNe that surround a Wolf-Rayet star, such as *Infinity*.

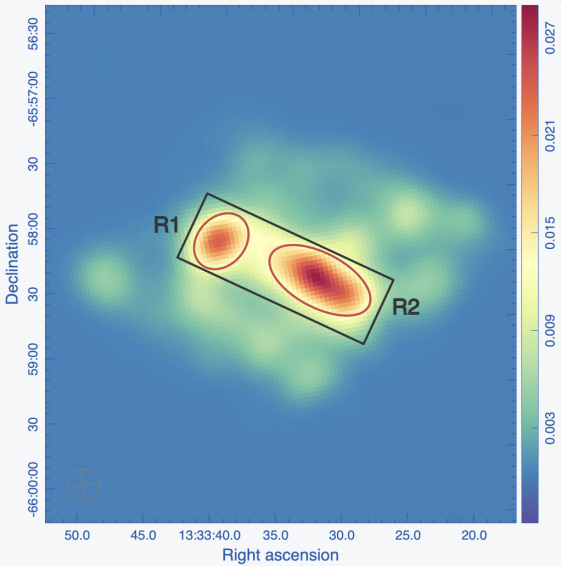

Figure 4. We outline in red the two inner envelopes in the central region of *Infinity* (which we arbitrarily identify as regions R1 and R2), from which we measure the respective integrated flux densities. Additionally, we measure the apparent size of the inner region containing R1 and R2, as outlined by the central black rectangle.

4. SUMMARY

Our motivation for this study has been to contribute radio continuum measurements for the well-known Galactic planetary nebula NGC 5189 (which we refer to colloquially as *Infinity*), using the ASKAP radio telescope array. The ASKAP-EMU survey has observed *Infinity* at 943 MHz, from which we have measured the integrated flux density, spectral luminosity, surface brightness, physical diameters, optical depth and electron column density. We also measured the integrated flux densities of *Infinity* in the SUMSS and PMN data, and combined those with other published radio measurements to determine the most up-to-date spectral index. We infer that *Infinity* is a thermal (free–free) emitting nebula, is in agreement with previous studies, and consistent with the expectations of a PNe composed of ionised plasma.

Acknowledgments We are grateful for the useful comments and suggestions made by Sanja Lazarević, Velibor Velović, Denis Leahy, and to our referee, which have improved the manuscript. This scientific work uses data obtained from Inyarrimanha Ilgari Bundara, the CSIRO Murchison Radio-astronomy Observatory. We acknowledge the Wajarri Yamaji People as the Traditional Owners and native title holders of the Observatory site. CSIRO's ASKAP radio telescope is part of the Australia Telescope National Facility. Operation of ASKAP is funded by the Australian Government with support from the National Collaborative Research Infrastructure Strategy. ASKAP uses the resources of the Pawsey Supercomputing Research Centre. Establishment of ASKAP, Inyarrimanha Ilgari Bundara, the CSIRO Murchison Radio-astronomy Observatory and the Pawsey Supercomputing Research Centre are initiatives of the Australian Government, with support from the Government of Western Australia and the Science and Industry Endowment Fund.

ADA is proudly supported by the Australian Government Research Training Program (RTP) Scholarship and CSIRO ATNF Space and Astronomy Student Program.

This research is also based on observations made with the NASA/ESA Hubble Space Telescope obtained from the Space Telescope Science Institute, which is operated by the Association of Universities for Research in Astronomy, Inc., under NASA contract NAS 5–26555. These observations are associated with program 12812.

References

Aller, A., Lillo-Box, J., Jones, D., Miranda, L. F., & Forteza, S. B. 2020, Astronomy & Astrophysics, 635, A128

Aller, L. H., & Milne, D. 1972, Australian Journal of Physics, 25, 91

Asher, A., Filipović, M., Bojičić, I., et al. 2024, Astrophysics and Space Science, 369, 85

Bains, I., Cohen, M., Chapman, J., Deacon, R., & Redman, M. 2009, Monthly Notices of the Royal Astronomical Society, 397, 1386

Barlow, M. 1987, Monthly Notices of the Royal Astronomical Society, 227, 161

Bear, E., & Soker, N. 2017, The Astrophysical Journal Letters, 837, L10

Bock, D.-J., Large, M., & Sadler, E. M. 1999, The Astronomical Journal, 117, 1578

Bojičić, I., Filipović, M., Urošević, D., Parker, Q., & Galvin, T. 2021, Monthly Notices of the Royal Astronomical Society, 503, 2887

Burger-Scheidlin, C., Brose, R., Mackey, J., et al. 2024, Astronomy & Astrophysics, 684, A150

Cerrigone, L., Umana, G., Trigilio, C., et al. 2017, Monthly Notices of the Royal Astronomical Society, 468, 3450

Chornay, N., & Walton, N. 2021, Astronomy & Astrophysics, 656, A110

Comrie, A., Wang, K.-S., Hsu, S.-C., et al. 2021, Astrophysics Source Code Library, ascl–2103

Condon, J., Broderick, J., & Seielstad, G. 1989, The Astronomical Journal, 97, 1064

Condon, J., Griffith, M. R., & Wright, A. E. 1993, The Astronomical Journal, 106, 1095

Cotton, W., Filipović, M., Camilo, F., et al. 2024, Monthly Notices of the Royal Astronomical Society, 529, 2443

Cozens, G., Walsh, A., & Orchiston, W. 2010, Journal of Astronomical History and Heritage, 13, 59

Crawford, E. J. 2015, PhD thesis, Western Sydney University

Crowther, P., De Marco, O., & Barlow, M. 1998, Monthly Notices of the Royal Astronomical Society, 296, 367

https://doi.org/10.1017/pasa.2025.10058 Published online by Cambridge University Press

Danehkar, A., Karovska, M., Maksym, W. P., & Montez, R. 2018, The Astrophysical Journal, 852, 87

Dunlop, J. 1828, Philosophical Transactions of the Royal Society of London, 118, 113

Evans, D. S., & Thackeray, A. D. 1950, Monthly Notices of the Royal Astronomical Society, 110, 429

Filipović, M., Cohen, M., Reid, W. A., et al. 2009, Monthly Notices of the Royal Astronomical Society, 399, 769

Filipovic, M. D. 1996, PhD thesis, University of Western Sydney, Australia

Filipović, M. D., Payne, J. L., Alsaberi, R., et al. 2022, Monthly Notices of the Royal Astronomical Society, 512, 265

Filipović, M. D., Dai, S., Arbutina, B., et al. 2023, The Astronomical Journal, 166, 149

Filipović, M. D., Lazarević, S., Araya, M., et al. 2024, Publications of the Astronomical Society of Australia, 41, e112

Filipovic, M. D., Smeaton, Z. J., Kothes, R., et al. 2025, Publications of the Astronomical Society of Australia, in press

Gathier, R., Pottasch, S., & Pel, J. 1986, Astronomy & Astrophysics, 157, 171

Gathier, R., Pottasch, S. R., Goss, W. M., & van Gorkom, J. H. 1983, Astronomy & Astrophysics, 128, 325

Gesicki, K., Zijlstra, A. A., & Miller Bertolami, M. M. 2018, Nature Astronomy, 2, 580

Gooch, R. 1996, Astronomical Data Analysis Software and Systems V, 101, 80

Griffith, M. R., & Wright, A. E. 1993, Astronomical Journal, 105, 1666

Gruenwald, R., & Aleman, A. 2007, Astronomy & Astrophysics, 461, 1019

Guzman, J., Whiting, M., Voronkov, M., et al. 2019, Astrophysics Source Code Library, ascl–1912

Hajduk, M., van Hoof, P. A., Śniadkowska, K., et al. 2018, Monthly Notices of the Royal Astronomical Society, 479, 5657

Hajduk, M., van Hoof, P. A., Zijlstra, A. A., et al. 2024, Astronomy & Astrophysics, 688, L21

Hopkins, A. M., Kapinska, A., Marvil, J., et al. 2025, The Evolutionary Map of the Universe: A new radio atlas for the southern hemisphere sky, arXiv:2505.08271

Hotan, A., Bunton, J., Chippendale, A., et al. 2021, Publications of the Astronomical Society of Australia, 38

Johnston, S., Taylor, R., Bailes, M., et al. 2008, Experimental Astronomy, 22, 151

Kwok, S. 2001, in Post-AGB Objects as a Phase of Stellar Evolution: Proceedings of the Toruń Workshop held July 5–7, 2000, Springer, 3–10

Kwok, S. 2005, Journal of the Korean Astronomical Society, 38, 271

Lazarević, S., Filipović, M. D., Koribalski, B. S., et al. 2024, Research Notes of the AAS, 8, 107

Leckrone, D., Cheng, E., Feinberg, L., et al. 1998, in American Astronomical Society Meeting Abstracts #192, Vol. 192, 35–08

Leverenz, H., Filipović, M. D., Bojičić, I. S., et al. 2016, Astrophysics and Space Science, 361, 108

Manick, R., Miszalski, B., & McBride, V. 2015, Monthly Notices of the Royal Astronomical Society, 448, 1789

Mari, M. B., Akras, S., & Gonçalves, D. R. 2023, Monthly Notices of the Royal Astronomical Society, 525, 1998

Marinelli, M., & Green, J. 2024, Wide Field Camera 3 Instrument Handbook, Version 17.0 (Baltimore: STScI)

Marr, J. M., Snell, R. L., & Kurtz, S. E. 2015, Fundamentals of radio astronomy: observational methods (CRC Press)

Mauch, T., Murphy, T., Buttery, H., et al. 2003, Monthly Notices of the Royal Astronomical Society, 342, 1117

Mezger, P., & Henderson, A. 1967, Astrophysical Journal, 147, 471

Mills, B. 1981, Publications of the Astronomical Society of Australia, 4, 156

Milne, D. 1979, Astronomy & Astrophysics Supplement Series, 36, 227

Milne, D., & Aller, L. H. 1975, Astronomy and Astrophysics, 38, 183

Milne, D. K., & Aller, L. H. 1982, Astronomy & Astrophysics, Supplement, 50, 209

Miszalski, B., Acker, A., Parker, Q., & Moffat, A. 2009, Astronomy & Astrophysics, 505, 249

Murphy, T., Mauch, T., Green, A., et al. 2007, Monthly Notices of the Royal Astronomical Society, 382, 382

Norris, R. P., Hopkins, A. M., Afonso, J., et al. 2011, Publications of the Astronomical Society of Australia, 28, 215

Pennock, C. M., van Loon, J. T., Filipović, M. D., et al. 2021, Monthly Notices of the Royal Astronomical Society, 506, 3540

Pérez-Sánchez, A., Vlemmings, W., Tafoya, D., & Chapman, J. 2013, Monthly Notices of the Royal Astronomical Society: Letters, 436, L79

Phillips, J., & Reay, N. 1983, Astronomy and Astrophysics, 117, 33

Pottash, S. R. 1983, Planetary Nebulae: A Study of Late Stages of Stellar Evolution (Dordrecht: D. Reidel Publishing Co.)

Ridpath, I. 2018, A Dictionary of Astronomy (3 ed.) (Oxford University Press, Oxford)

Robertson, J. 1991, Australian Journal of Physics, 44, 729

Sabin, L., Vázquez, R., López, J., García-Díaz, M. T., & Ramos-Larios, G. 2012, Revista mexicana de astronomía y astrofísica, 48, 165

Sasaki, M., Zangrandi, F., Filipović, M., et al. 2025, A&A, 693, L15

Sault, R. J., Teuben, P., & Wright, M. C. 2011, MIRIAD: Multi-channel image reconstruction, image analysis, and display (Astrophysics Source Code Library), ascl–1106

Sault, R. J., Teuben, P. J., & Wright, M. C. 1995, Astronomical Data Analysis Software and Systems IV, 77, 433

Slee, O., & Orchiston, D. 1965, Australian Journal of Physics, 18, 187

Smeaton, Z. J., Filipović, M. D., Koribalski, B. S., et al. 2024a, Research Notes of the AAS, 8, 158

Smeaton, Z. J., Filipović, M. D., Lazarević, S., et al. 2024b, Monthly Notices of the Royal Astronomical Society, 534, 2918

Suárez, O., Gómez, J. F., Bendjoya, P., et al. 2015, The Astrophysical Journal, 806, 105

Tacchella, S., Smith, A., Kannan, R., et al. 2022, Monthly Notices of the Royal Astronomical Society, 513, 2904

Taylor, A., Pottasch, S., & Zhang, C. 1987, Astronomy & Astrophysics, 171, 178

Wilson, T. L., Rohlfs, K., & Hüttemeister, S. 2013, Tools of Radio Astronomy (6th ed.) (Springer)

Wright, A. E., Griffith, M. R., Burke, B., & Ekers, R. 1994, Astrophysical Journal Supplement Series, 91, 111

Zhang, Y., Liu, X.-W., Wesson, R., et al. 2004, Monthly Notices of the Royal Astronomical Society, 351, 935

Zijlstra, A. A., Van Hoof, P. A., Chapman, J. M., & Loup, C. 1994, Astronomy & Astrophysics, 290, 228

https://doi.org/10.1017/pasa.2025.10058 Published online by Cambridge University Press